Materials & Design 223 (2022) 111128

Contents lists available at ScienceDirect

Materials & Design

journal homepage: www.elsevier.com/locate/matdes

Multilayer Mo_2N-Ag/SiN_x films for demanding applications: Morphology, structure and temperature-cycling tribological properties

Hongbo Ju [a,b,*], Rui Zhou [a], Jing Luan [a], Lihua Yu [a], Junhua Xu [a,*], Bin Zuo [a], Junfeng Yang [c,*], Yaoxiang Geng [a], Lijun Zhao [a], Filipe Fernandes [b,d]

[a] School of Materials Science and Engineering, Jiangsu University of Science and Technology, Mengxi Road 2, Zhenjiang, Jiangsu Province 212003, China
[b] University of Coimbra, CEMMPRE-Centre for Mechanical Engineering Materials and Processes, Department of Mechanical Engineering, Rua Luís Reis Santos, Coimbra 3030-788, Portugal
[c] Key Laboratory of Materials Physic, Institute of Solid State Physics, Hefei Institute of Physical Sciences, Chinese Academy of Sciences, Hefei 230031, China
[d] ISEP - School of Engineering, Polytechnic of Porto, Rua Dr. António Bernardino de Almeida 431, 4200-072 Porto, Portugal

HIGHLIGHTS

- A multilayered architecture of Mo_2N-Ag and SiN_x nanolayers in Mo_2N-Ag/SiN_x films.
- Room temperature tribological properties were improved with increasing period thickness up to 64 nm.
- Multilayered Mo_2N-Ag/SiN_x films avoided the excessive diffusion of Ag at elevated temperatures.
- Inserting SiN_x layers avoided the excessive diffusion of Ag at high temperature.
- Multilayer films exhibited excellent temperature-cycling tribological properties.

GRAPHICAL ABSTRACT

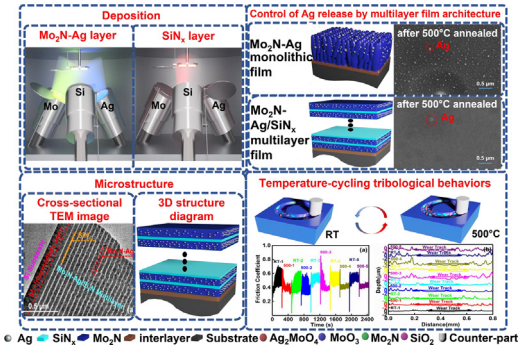

ARTICLE INFO

Article history:
Received 8 May 2022
Revised 16 August 2022
Accepted 6 September 2022
Available online 15 September 2022

Keywords:
Magnetron sputtering
Mo_2N-Ag/SiN_x multilayer films
Modulation period
Tribological properties
Temperature-cycling tribology

ABSTRACT

Nowadays there is the need to avoid the excessive consumption of liquid lubricant oils, as they are harmful to the environment and hard to disposal. Self-lubricant films have been seen as the sustainable solution to achieve a long-term lubrication under high temperature-cycling conditions. In this manuscript, multilayer Mo_2N-Ag/SiN_x films with a fixed modulation ratio (thickness of Mo_2N-Ag to SiN_x) of 3:1, with changing modulation period (Λ, thickness of Mo_2N-Ag and SiN_x) from 8 to 200 nm were produced to achieve an effective balance between the lubricious phase diffusion control and the adequate formation of the low friction tribo-layers. Results showed that a dual-phase of fcc-Mo_2N and fcc-Ag co-existed in Mo_2N-Ag layers, while the SiN_x layer exhibited an amorphous character. Both room temperature (RT) lubricant and wear-resistance properties of the films were improved by increasing Λ from 8 to 64 nm, while a further increase of Λ degraded the wear-resistance properties. The multilayer film at Λ = 64 n m exhibited an excellent RT-500 °C temperature-cycling tribological properties. Mechanical properties and the synergistic effect of both modulation layers were the cause for the improvement of the tribological properties.

© 2022 The Authors. Published by Elsevier Ltd. This is an open access article under the CC BY-NC-ND license (http://creativecommons.org/licenses/by-nc-nd/4.0/).

* Corresponding authors at: School of Materials Science and Engineering, Jiangsu University of Science and Technology, Mengxi Road 2, Zhenjiang, Jiangsu Province 212003, China.
E-mail addresses: hbju@just.edu.cn (H. Ju), jhxu@just.edu.cn (J. Xu), jfyang@issp.ac.cn (J. Yang).

https://doi.org/10.1016/j.matdes.2022.111128
0264-1275/© 2022 The Authors. Published by Elsevier Ltd.
This is an open access article under the CC BY-NC-ND license (http://creativecommons.org/licenses/by-nc-nd/4.0/).

1. Introduction

Friction is both an ancient and a young science, it has been affecting people's life all the time since the drilling wood for fire in ancient times to today's nano friction generators [1–5]. Seeking an anti-friction and wear-resistance solid material which can achieve an efficient and stable service of core components in the field of airplane engine, thermonuclear, tools and abrasives is a current hot topic in the field of materials [6–10]. With the increasingly stringent global energy conservation and emission reduction policies, improving the lubrication properties of workpiece surface in wide temperature range to realize "zero lubricating oil" or "micro oil lubrication" has significant science and research meaning and application value [11–15]. Therefore, during recent twenty years, a wide variety of solid lubricating films were produced and design by combining the intrinsic properties of some binary and ternary films which are very hard and resistant to oxidation, with specific elements which diffused up to the surface and formed a low friction tribolayer. Addition of soft metals such as Ag [16–20] and Cu [21–25], was observed to be one of the more efficient solutions to obtain self-lubrication properties at a wide temperature range. Nevertheless, the strong out-diffusion of the lubricious element and its quick depletion from the entire volume of the film only allows low friction behavior for short periods of time, leading after few minutes to the failure of the film [26–30]. For example, additions of Ag to Mo_2N hard films allows to improve their lubrication performance in a wide range of temperatures [31–34]. Similar results have been reported for Mo_2N-Cu films [35]. However, the excessive diffusion of Ag from the entire volume of the film to the surface of the films, leads after critical time to the failure of the films and consequently to higher wear rates at elevated temperatures [36]. Besides this, soft metals reduce the hardness of the films [37–41], also degrading their wear resistance properties.

Nano-multilayer architecture was reported to be an effective method to achieve the long-term wide-range temperature self-lubricant properties [42]. This design depending on the layer materials is able to (i) inhibit the heat flows induced by the frictional heat sources during the wear test [43–45], (ii) work as a barrier layer to avoid the strong diffusion of soft metal to the surface [46–48] and (iii) enhance the wear-resistance by changing the wear mechanism due to the formation of the transition zones between the adjacent layers, which can hinder crack propagation or even relax them [49] and (iv) increase hardness if the superlattice effect is reached [27]. Barrier layers have been applied to avoid the strong diffusion of soft metal to the surface and thus achieve the long-term self-lubrication properties at wide range of temperatures. For example, J. Hu et al. [50] deposited a 300 nm TiN top layer over a YSZ-Ag-Mo self-lubricant films and results confirmed that the top barrier layer could enhance the wear-resistance at 500 °C. Beyond this, a TiN barrier layer was also used to produce a YSZ-Ag-Mo/TiN multilayer film with 2, 4, and 8 TiN layers, resulting in an excellent temperature-cycling tribological properties of those films [51]. The multilayer design could be thus considered as an effective method to avoid the excessive diffusion of soft metals during the wear testing [52–54]. Soft metals mainly diffuse from inner part of the film to the surface though the grain boundaries [55]. Hence, amorphous phases with excellent thermal stability and mechanical properties combined in a multilayer configuration with a hard matrix alloyed with the lubricious element could be the solution to extend the long-term self-lubricant properties of the self-lubricant films. In this paper, amorphous SiN_x phase with excellent oxidation resistance (~1200 °C) and higher hardness (~21 GPa) was chosen as a barrier layer to control the diffusion of the lubricious phase in the Mo_2N-Ag films. Therefore, the present research work aims to investigate the influence of the modulation period on the microstructure, mechanical properties and essentially tribological properties at room temperature and temperature-cycling conditions (cycle RT-500 °C repeated different times).

2. Experimental details

Series of Mo_2N-Ag/SiN_x nano-multilayer films were prepared using RF magnetron sputtering system, using high purity (99.9%) Mo, Si and Ag targets. The 3D schematic representation of the deposition system and the films configuration are illustrated in Fig. 1. Polished high-speed steel W18Cr4V (W18) and Si (100) wafers were used as substrates in the depositions. Before depositions the substrates were ultrasonically cleaned in alcohol for 15 min and propanol for 15 min. High-speed steel substrates were used for mechanical properties evaluation (Hardness and elastic modulus and tribological assessment, either at room temperature (RT) and temperature cycling conditions (RT-500 °C, repeated different times), whilst, Si substrates were used for XRD, XPS and TEM analysis. The distance between the targets and substrates was set to 80 mm. Prior the depositions, the chamber was vacuum down below 6.0×10^{-4} Pa. A Mo adhesion layer with thickness ~ 150 nm was firstly deposited under Ar flow of 10 sccm in order to improve the adhesion of the films to the substrate. After that, the multilayer structure was deposited by opening the Mo and Ag shutters and closing the shutter of the Si target, in alternated way, in the presence of a N_2 atmosphere. The multilayered structure was growth by applying a power 280, 150 and 50 W at the Mo, Si and Ag targets, respectively, in all the depositions. The Ar and N_2 partial pressures were 0.23 and 0.7 Pa, corresponding to a total working pressure of 0.3 Pa. Films with different modulation periods ranging from 8 to 200 nm with a fixed thickness ratio of Mo_2N-Ag to SiN_x of 3:1, were produced by controlling the sputtering time of Mo, Ag and Si targets. Reference Mo_2N-Ag and SiN_x monolayer films were also deposited under the same deposition conditions to infer about the individual layers composition and chemical bonding.

The elemental chemical composition of reference Mo_2N-Ag and SiN_x monolayers was analyzed by an energy dispersive spectrometer (EDS, Oxford, UK). The structure of Mo_2N-Ag/SiN_x films was determined by X-Ray diffraction (XRD, Shimazu-6000, Shimadzu, Kyoto, Japan) with Al kα irradiation at a pass energy of 160 eV, and 2θ was in the range of 20-80° with a step of 0.4°. The valence states of elements were investigated by X-ray photoelectron spectroscopy (XPS, ESCALAB250XI, Thermo Fisher, USA). The Spectrum of C 1s with bonding energy of 284.8 eV was used for calibration. Before measurements the surface of the specimens were bombarded with a gentle Ar^+ ions (primary energy of 800 eV at an angle of ~70° from the surface normal) for 30 s, to remove the surface contaminants. The microstructure of films was investigated by the transmission electron microscope (TEM, JEOL, JEM-2100F, Japan). Hardness (H) and elastic modulus (E) was measured by a nano-indentation (Anton Paar, CPX + NHT2 + MST, Switzerland), setting the constant loading force to 3 mN and holding time of 10 s. In order to ensure the accuracy of the results 15 measurements were done in 2 different zones of the specimens. The room temperature (RT) wear tests were conducted in a pin-on-disc tester (UMT-2, CETR, USA) using alumina balls (diameter of 9.4 mm) as counterpart, in open air. The radius of track was 4 mm, the applied load was 3 N, the rotation speed was 50 rpm and the sliding time was 20 min. The relative humidity during all the testes was ~30%. Selected films (Mo_2N-Ag monolayer film and multilayered Mo_2N-Ag/SiN_x film with period thickness of 64 nm) were also tested under temperature-cycling conditions (RT-500 °C) with a cycle of 5 repetitions, carried out under the same experimental conditions

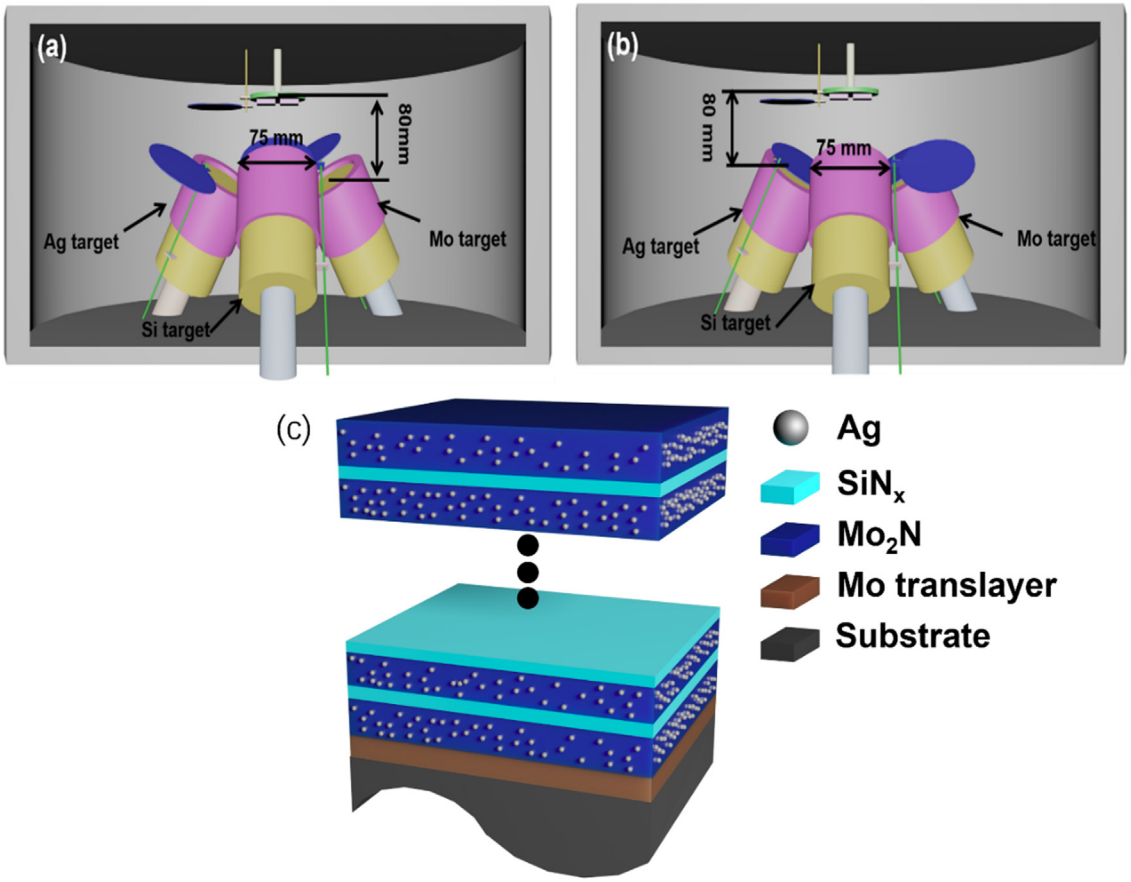

Fig. 1. 3D schematic representation of the deposition chamber: (a) shutters in front of the Mo and Ag targets opened to deposit the Mo_2N-Ag layer, (b) shutter at the Si target opened and at the Mo and Ag targets closed to deposit the SiNx layer, (c) 3D representation of the multilayer Mo_2N-Ag/SiN_x films.

as for RT. The average friction coefficient of films after the wear tests was taken from the steady state zone of their corresponding friction curves. The 2D profiles of the wear tracks was measured by the 3D Profiler (BRUKER, Dektak-XT, Germany), and the wear rate of the films obtained using Archard's law. SEM and Raman spectrometer (inVia, Renishaw, UK) were applied to measure the wear track surface and the tribo-phase on the wear track respectively.

3. Results and discussion

3.1. Microstructure

Fig. 2 illustrates the XRD diffraction patterns of reference monolithic Mo_2N-Ag and SiNx layers and Mo_2N-Ag/SiN_x multilayer films with different modulation periods (Λ). The XRD pattern of Mo_2N-Ag monolayer film exhibits diffraction peaks assigned to fcc-Mo_2N, fcc-Ag, pure molybdenum from the transition layer, and silicon substrate. This result confirms that a dual-phase of fcc-Mo_2N and fcc-Ag co-exists in the Mo_2N-Ag monolayer film. Soft metals, such as Ag and Cu, were widely incorporated into the hard nitride based films to induce the lubricant performance, and have been reported to be insoluble on the nitride matrix [56–60]. Excluding the substrate contribution (peaks at ~34° and ~70° assigned to silicon), no diffraction peak could be indexed to the monolithic SiN_x layer. This is an expected result as SiN_x phase have been reported to display an amorphous character. EDS Analysis conducted at the monolithic layers revealed that the ratio Ag/(Mo + N + Ag) in the monolithic Mo_2N-Ag layer is ~26.4 at.%, and oxygen in the film

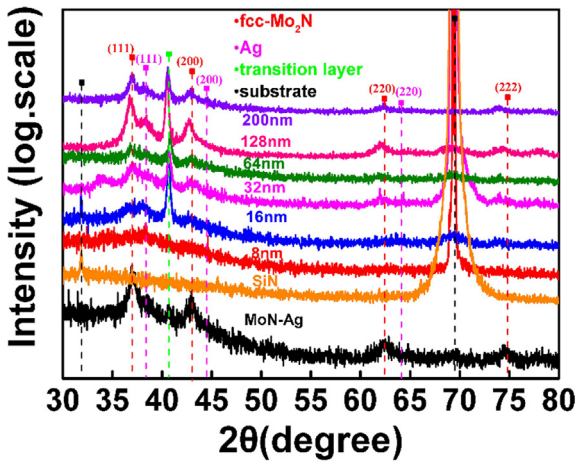

Fig. 2. XRD diffraction patterns of Mo_2N-Ag monolayer film, SiN_x monolayer film, and Mo_2N-Ag/SiN_x multilayer films as function of modulation periods.

was ~3.2 at.%. Si, N and O contents in the monolithic SiN_x layer was ~45.3, ~50.5, and ~4.2 at.% respectively. The multilayer film with 8 nm period thickness displayed a broaden peak with very low intensity at ~36-40°. As suggested the diffraction peaks of the individual monolithic layers, the barely visible diffraction peaks corresponds to the diffraction peaks of fcc-Mo_2N and fcc-Ag phases. The small period thickness of the multilayer should be the cause for the poor crystal quality of the Mo_2N-Ag layers. Increasing Λ leads to the appearance of well defined diffraction

peaks, which are similar from the ones of the Mo_2N-Ag monolayer film.

High-resolution XPS spectra of Mo_2N-Ag and SiN_x monolayer films are shown in Fig. 3. As shown in Fig. 3(a), two peaks at ~231.8, ~232.4 eV can be indexed at the Mo 3d spectrum of Mo_2N-Ag monolayer film. The first one belongs to the Mo-N bonds in Mo_2N, and the other one refers to Mo-O bonds in molybdenum oxide phase [61]. Four peaks at ~368.4, ~368.6, ~374.4 and ~374.8 are detected in the Ag 3d spectrum from the Mo_2N-Ag monolayer film (Fig. 3b), corresponding to Ag-Ag bonds in metal

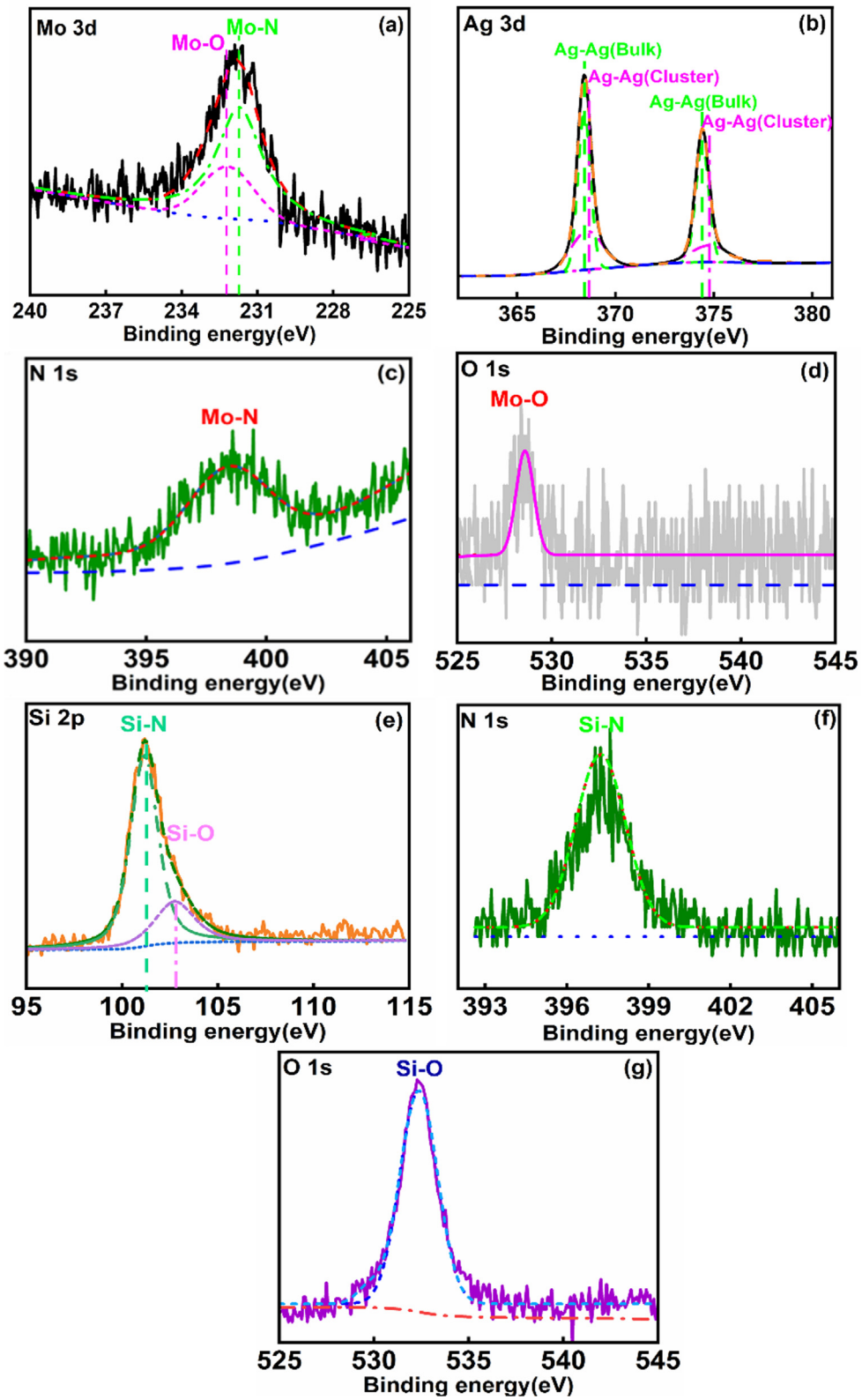

Fig. 3. High-resolution XPS spectra of Mo 3d (a), Ag 3d (b), N 1s (c) and O 1s (d) for Mo_2N-Ag monolithic film, and Si 2p (e), N 1s (f), O 1s (g) for SiN_x monolithic film.

silver [41]. N 1s spectrum of the monolithic film exhibits a single peak at ~398.3 eV, corresponding to Mo-N bonds in Mo_2N [61], as shown in Fig. 3(c). O 1s of the monolayer sample is shown in Fig. 3(d), and a peak at ~530.5 eV corresponds to Mo-O bonds in molybdenum oxide phase [62], as also detected in the Mo 3d spectrum. Si 2p spectrum of monolayer SiN_x film, shown in Fig. 3(e), exhibits two peaks at ~100.8 and ~102.7 eV, which refers to the bonding energy of Si-N in amorphous SiN_x (~101.8 eV) [63] and Si-O in SiO_2 phase [64], respectively. As for the N 1s spectrum of the SiN_x sample, an obvious peak at ~397.3 referring to Si-N bonds in amorphous SiN_x is detected. Single peak at ~398.2 eV is detected in the O 1s spectrum of SiN_x monolayer film, which could be described as the Si-O bonds in SiO_2 oxide [65]. Hence, Mo_2N, Ag and residual MoO_3 phases co-exists in the Mo_2N-Ag monolayer film, whilst, SiN_x and residual Si-O phases co-exists in the SiN_x monolithic film.

Fig. 4 shows the cross-sectional TEM image and the corresponding SAED pattern of the Mo_2N-Ag/SiN_x multilayer film with Λ of 64 nm. The cross-sectional TEM image in Fig. 4(a), clearly shows the architecture of the produced films, including the substrate (silicon wafer), adhesion layer of molybdenum, Mo_2N-Ag and SiN_x modulation layers. The SAED diffraction pattern includes two sets of diffraction rings corresponding to fcc-Mo_2N and fcc-Ag phases, as shown in Fig. 4(b). The diffraction rings corresponding to fcc-Mo_2N (111) and (200) are continuous, while the ones for fcc-Ag are discontinuous. This might be attributed by the size and distribution of both crystal phases (see Fig. 4d). Soft metal phases of Ag or Cu were observed to be fine distributed in TiN and Mo_2N matrixes as observed by HRTEM in our previous results [35,66]. No diffraction rings, referring to silicon or silicon nitride phase, appears in the SAED pattern, strengthens the presence of amorphous SiN_x phase in the Si-N layer. Magnification TEM image of as-deposited multilayer film is shown in Fig. 4(c). Mo_2N-Ag layer is darker than the SiN_x one due to the different electron scattering factors. A modulation period of ~64 nm is observed, with the thickness of Mo_2N-Ag and SiN_x modulation layers of ~48 and ~16 nm, respectively. Modulation ratio of Mo_2N-Ag to SiN_x is ~3:1 based on above results, in good agreement with the design architecture. HRTEM is also displayed in Fig. 4(d) to further detail the microstructure of each modulation layer. A clear interface between the Mo_2N-Ag and SiN_x layers is detected. However, two sets of lattice fringe appear in the Mo_2N-Ag layer: one corresponds to fcc-Mo_2N (111) with a lattice spacing of ~0.246 nm (JCPDF card # 24-0768), and other of fcc-Ag (111) with lattice parameter of ~0.228 nm (JCPDF card # 65–2871). Both FFT patterns from Mo_2N and Ag phases also exhibit a single cubic diffraction spots. In addition, the lattice fringe corresponding to fcc-Mo_2N (111) occupy most space of the Mo_2N-Ag layer, and defects are almost nonexistent. Obvious distorted lattice fringes are detected in the fcc-Ag phase. This might result in the observed discontinuity of diffraction rings of Ag phase in the SAED pattern as shown previously.

In conclusion, and in good agreement with XRD and XPS results, TEM analysis confirmed the formation of a multilayered architecture altering Mo_2N-Ag and SiN_x layers. The Mo_2N-Ag layer exhibited a dual-phase of fcc-Mo_2N and fcc-Ag, and the SiN_x layer was an amorphous phase.

3.2. Mechanical and tribological properties

Hardness (H) and elastic modulus (E) of the Mo_2N-Ag/SiN_x multilayer films are illustrated in Fig. 5. The increase of the Λ from 8 to

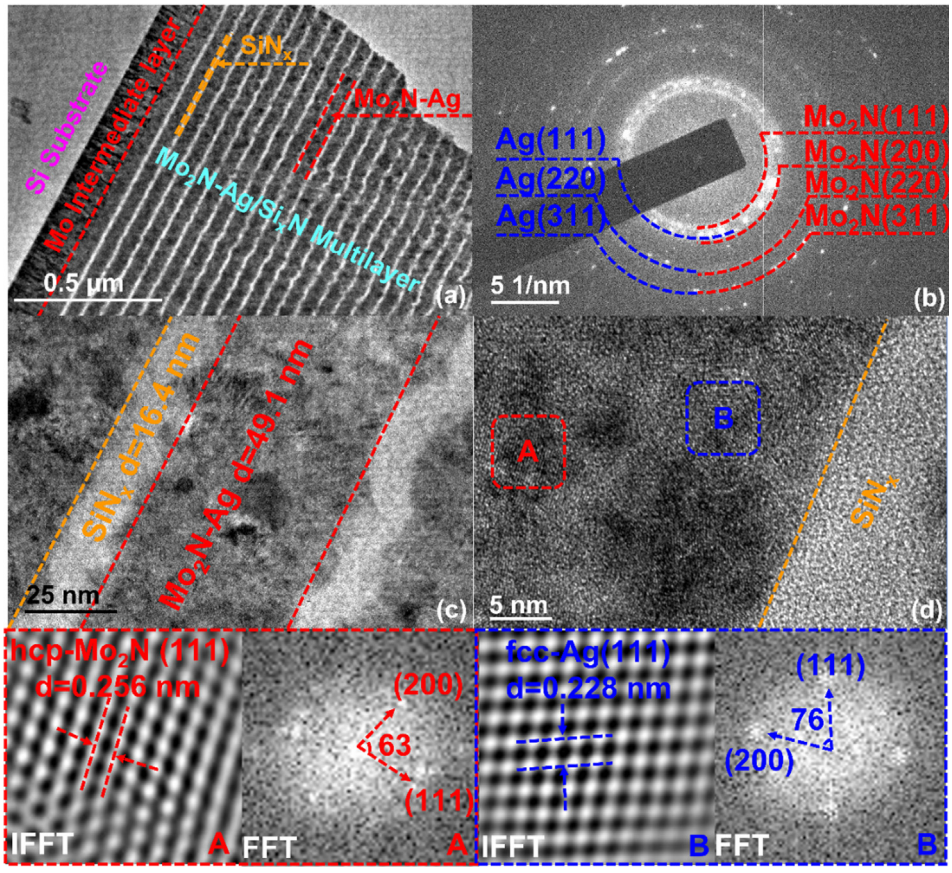

Fig. 4. (a) Cross-sectional TEM image of multilayered Mo_2N-Ag/SiN_x films with period thickness of 64 nm, (b) corresponding SAED patterns, (c) magnified TEM image and (d) HRTEM image.

64 nm does not significantly change the hardness of the multilayer films, being ~13 GPa. Further increase of the Λ to 128 nm drops the hardness to ~8 GPa, and then the further increase of the Λ to 200 nm does not further significantly changes the hardness value. A Λ of 8–128 nm exhibits a little effect on the elastic modulus, holding a stable value of ~200 GPa, while a further increase of Λ increases the elastic modulus to ~300 GPa. The hardness and elastic modulus measured for the monolithic Mo_2N-Ag and SiN_x films are H= ~11 GPa and E= ~240 GPa; and H= ~21 and E= ~120 GPa, respectively. In many materials combinations, the evolution of the hardness as a function of the period thickness have shown a characteristic behavior, with maximum hardness values normally obtained for a period thickness in the range of 2–10 nm [67]. Such high hardness is reported to occur by the blocking dislocations motion at the layer interfaces, owing to the differences in the shear moduli of the individual layers and by coherency strain causing periodical strain–stress fields in the case of lattice mismatched multilayered films. Further increase of multilayer films thickness decreases the hardness of the films and for a certain threshold period thickness multilayers the hardness of the films starts to be represented by the weighted average of the hardness of the individual layers. Thus, the lower hardness and elastic modulus of the films can be interpreted based on the high period thickness of the multilayers structure, which avoids the establishment of the superlattice effect. The hardness of the coatings are thus represented by the weighted average of the individual layers. This justifies the stable values of hardness (~13 GPa) and elastic modulus (~200 GPa) of multilayered films with a Λ of 8–64 nm. Further increase in Λ to above 128 nm drops the value of hardness and elastic modulus. It should be highlight that top layer of all as-deposited multilayer films is the Mo_2N-Ag layer, which considering the depth penetration of the indenting tests (~150 nm) represents the hardness of the monolithic Mo_2N-Ag film.

Fig. 6 illustrates the RT average friction coefficient (Cof.) and wear rate (WR) of the Mo_2N-Ag/SiN_x multilayer films with various modulation periods. Cof. value firstly drops gradually from ~0.56 at Λ of 8 nm to ~0.50 at Λ of 64 nm, and then holds stable Cof. with a further increase of Λ. However, significant change on the WR can be observed with the increase of the modulation period. The WR progressively drops with increasing Λ up to 64 nm to $\sim 5 \times 10^{-5}$ mm^3/N.mm and then WR increases with a further increase in Λ.

Fig. 7 illustrates the RT wear track morphology of the multilayer films as a function of modulation periods. Huge amounts of ploughings accompanying with an obvious desquamation and deep scratch in some area of the wear track surface of the film with a Λ of 12 nm are detected, as shown in Fig. 7(a). Increasing Λ to 96 nm could enhance the tribological performance based on the results from Fig. 7(b) of narrowed wear track and disappearance of film desquamation, though there are still some deep scratches. Further increase of the Λ to 200 nm induces large amount of debris on the wear track and disappears deep scratches. But the obvious ploughings are still detected as shown in Fig. 7(c).

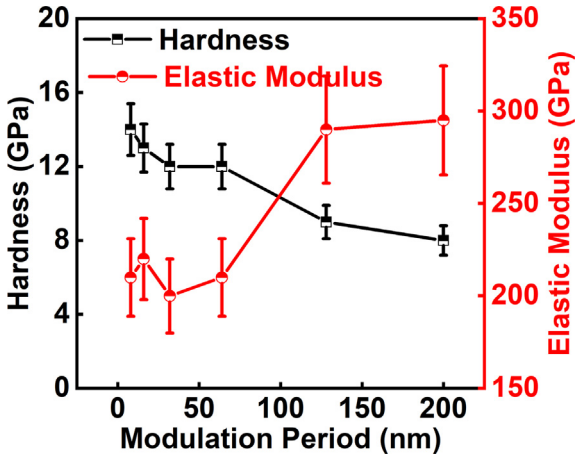

Fig. 5. Hardness and elastic modulus of the Mo_2N-Ag/SiN_x multilayer films with various modulation periods.

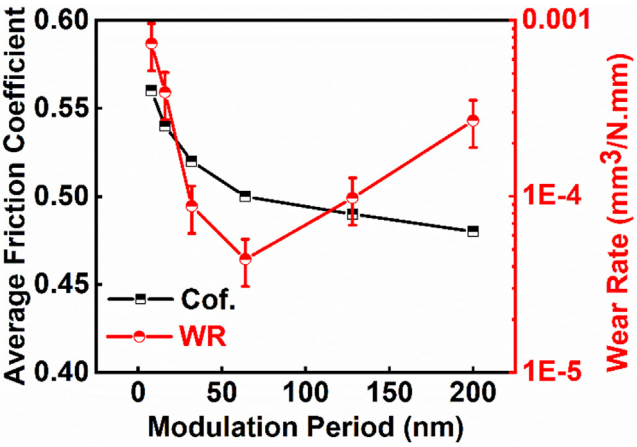

Fig. 6. Room temperature (RT) average friction coefficient (Cof.) and wear rate (WR) of Mo_2N-Ag/SiN_x multilayer films with various modulation periods.

Two main factors can help explain the RT Cof. and WR values variations: (i) role of each modulation layer. The lubricant property of the multilayer films is mainly ensured by the Mo_2N-Ag layer. Both Ag and Mo_2N phases are accepted traditional solid lubricants and are reported to exhibit excellent lubricant performance during the wear test at RT [68,69]. Additionally, the Ag_2MoO_4 phase detected on the wear track (see Raman spectra of the wear track at temperature-cycling conditions) is working as lubricant phase as well, as demonstrated by D. Wang et al. [70]. Enhancement on the hardness of the Mo_2N-Ag layer by inserting hard SiN_x could improve the capabilities of load-bearing (hardness) during the wear test at RT. (ii) synergistic effect between both modulation layers. Thickness of each modulation layer plays an important role in this part. Alumina counterpart first contacts with the top layer of Mo_2N-Ag. The top layer could provide a relative low Cof at the beginning of the wear test, but it exhibits high WR due to its low hardness and formation of layered tribo-phase [62,66]. The brittle SiN_x layer will be continuously exposed to the counterpart after the worn out of the Mo_2N-Ag layers, and will form hard debris under the shear force and downforce. The hard debris from SiN_x layer could scratch the self-lubricant layer of Mo_2N-Ag, and the wear rate is furtherly exacerbated.

Based on the factors referred above, two stages could be divided according to the tendency of Cof. and WR: (i) one is the continuous reduction in both Cof. and WR, corresponding to the film with a Λ below 64 nm. At this period, the lubricant behavior is enhanced by the increase of the Mo_2N-Ag layer thickness, and this results in the continuous reduction in Cof. Continuous lubrication also drops the WR with the increase of Λ, since the film exhibits a relative high value in hardness (~12 GPa) and H/E ratio (~0.6). (ii) continuous increase in WR with a stable value of Cof., corresponding to the film with a Λ above 64 nm. Although the Mo_2N-Ag layer could provide the lubricant phases to remain the Cof stable, it also weakens the mechanical properties, consequently degrading the wear performance. Beyond this, hard debris from the SiN_x layer could be considered to be increased with the increase of SiN_x layer thickness. This also contributes to the increase of the WR at this period.

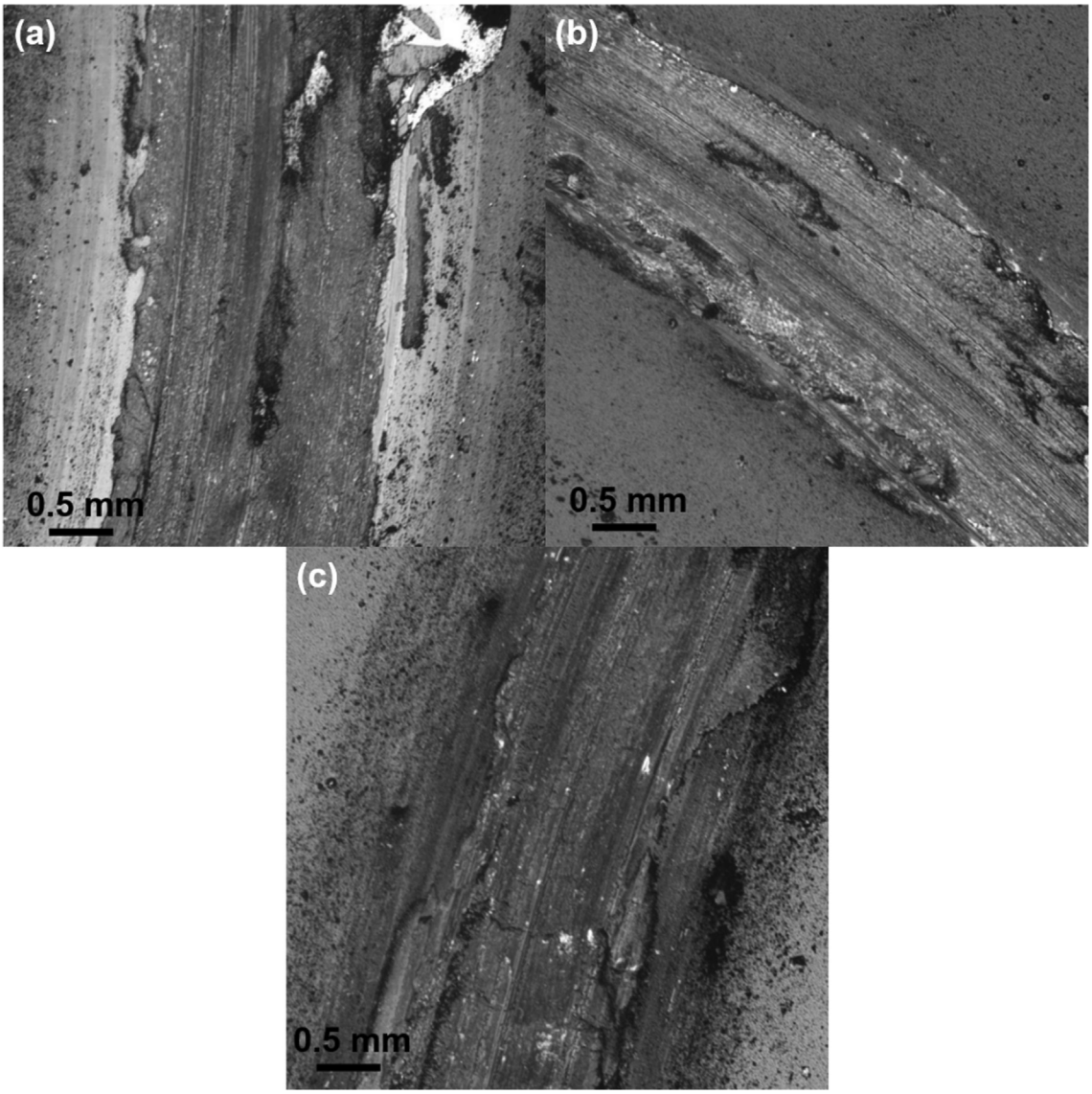

Fig. 7. Wear track morphology of the multilayer films as a function of modulation periods: (a) 12, (b) 96 and (c) 200 nm.

Inserting SiN_x layers into the Mo_2N-Ag matrix to synthesize a multilayer film with a Λ of 64 nm (the thickness of Mo_2N-Ag and SiN_x is ~48 and ~16 nm respectively) could improve the RT tribological properties, and exhibits the tremendous application potential as self-lubricant hard films coated on the surface of cutting tools, moulds and engine pistons to prolong life, reduce energy consumption. However, temperature-cycling is often involved regarding to the actual working conditions of high-speed and dry cutting, open/close action of moulds, and the auto start and stop of engines [71–73]. The temperature-cycling tribological properties of the multilayer film with a Λ of 64 nm was also evaluated, and the friction curves and 2D wear track profiles after every temperature-cycling conditions are shown in Fig. 8. Samples was first tested at RT (RT-1), and then the temperature was increase to 500 °C to carry out the high temperature tribological test (500–1). RT-1 + 500–1 is defined as the first temperature-cycling wear test unit. Then temperature-cycling wear test was repeated until unit 5, and all temperature-cycling wear tests were carried out at the same wear track. As shown in Fig. 8(a), all friction curves regardless of testing temperatures include two main stages, one is running-in and the other is the steady state stage. RT friction coefficient of the sample regardless of the number of temperature-cycling does not significantly varies. The same can be observed for 500 °C friction coefficient of the films from the five temperature-cycling wear test units. The 2D wear track profiles at the RT-500 °C temperature-cycling conditions is shown in Fig. 8(b). Results confirms an excellent wear-resistance after the five RT-500 °C temperature-cycling wear tests as the maximum wear depth is below 2 μm. The wear track seems relative smooth and small amount of wear debris have seen to be accumulate on both sides of the wear track after the RT-1 wear test. A rough wear track surface is detected with an obvious debris accumulation on the wear track sides for the sample at 500–1. Then a smooth wear track surface also appears after the RT-2 wear test, and the 500–2 wear test induces the rough wear track surface again. Therefore, polishing wear might be the main wear mechanism at RT, whilst, oxidation and abrasive wear could be considered as the main wear mechanism at 500 °C. Cof. and WR of the sample under the RT-500 °C temperature-cycling conditions is shown in Fig. 8(c) and (d). All Cof. values at RT remain at approximately to 0.5, and ones at 500 °C at ~0.4. As for WR under the temperature-cycling conditions, the value increases gradually with the increase of

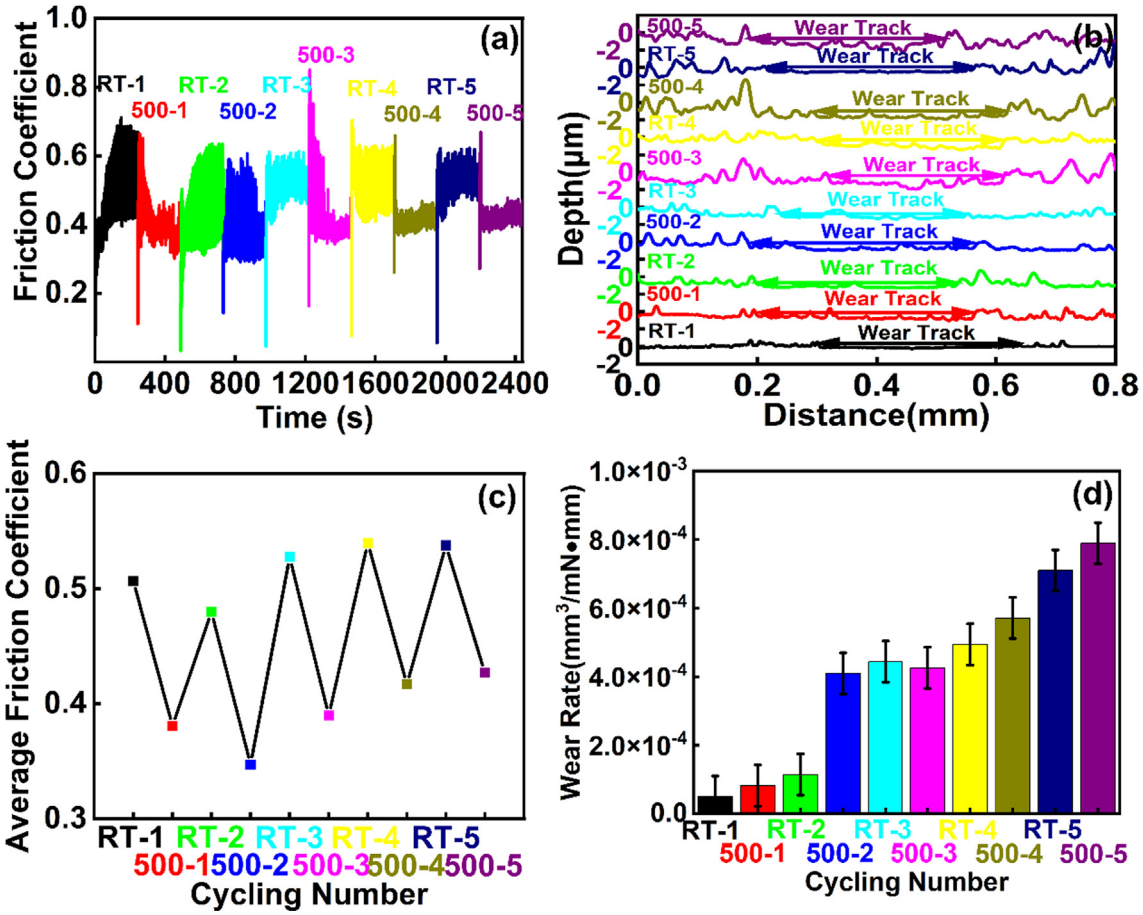

Fig. 8. (a)Friction curves, (b) 2D wear track profiles, (c) average friction coefficient f and (d) wear rate of the Mo_2N-Ag/SiN_x multilayer film with Λ = 64 nm under the RT-500 °C temperature-cycling conditions.

temperature-cycling numbers. The Mo_2N-Ag monolayer film with a thickness of 2 μm was also tested at temperature cycling conditions, and the results showed that the film was worn out at RT-2. The excessive diffusion of silver phase from inner to the film surface through the grain boundaries at elevated temperature revealed to be the cause for the failure of the film (see Fig. 10).

Yield strength of the as-deposited multilayer films is widely considered to be equal or approximately equal to one third of its hardness [74]. The contact pressure in the tribological contact, considering the applied load can be estimated as ~0.27 ± 0.1 GPa under the RT-500 °C temperature-cycling conditions, and it is lower than the yield strength. Hence, the main factors attributing to the Cof. and WR as a function of temperature-cycling conditions is the surface interaction between wear track surface and counterpart, since the multilayer film system chosen to investigate the temperature-cycling tribological behaviors exhibits the same mechanical properties.

Due to the sliding movement of the ball combined with the testing temperature and friction tribo-phases will be generated on the contact [75]. The Raman spectra from the wear track surface after RT-1 and 500–1 wear test is shown in Fig. 9. Three main tribo-phases (Ag_2MoO_4, SiO_2 and MoO_3) are detected in the Raman spectrum from the RT-1 wear track. Raman spectrum from the 500–1 wear track confirms that similar tribo-phases (SiO_2, MoO_3 and Ag_2MoO_4) exist in the wear track surface, and the intensity of Raman peaks is higher than that from RT-1. Further increase of the testing temperature increases the relative content of the same tribo-phases. The lubricant properties of MoO_3 has been widely discussed for nearly two decades and have seen the responsible for

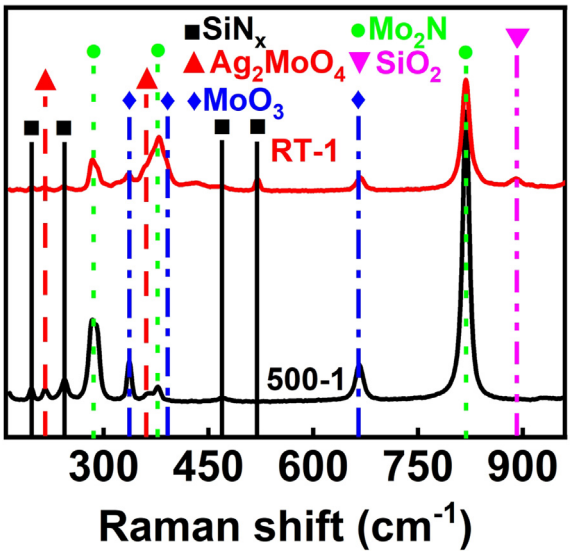

Fig. 9. Raman spectra of wear track surface of the films at RT-1 (a) and 500–1 (b).

the self-lubritious properties in the sliding contacts. Ag_2MoO_4, also reported to exhibit self-lubricant property at elevated temperatures [70]. Thus, the presence of this phase on the sliding contact is the responsible for the good tribological performance of the films under cycling conditions.

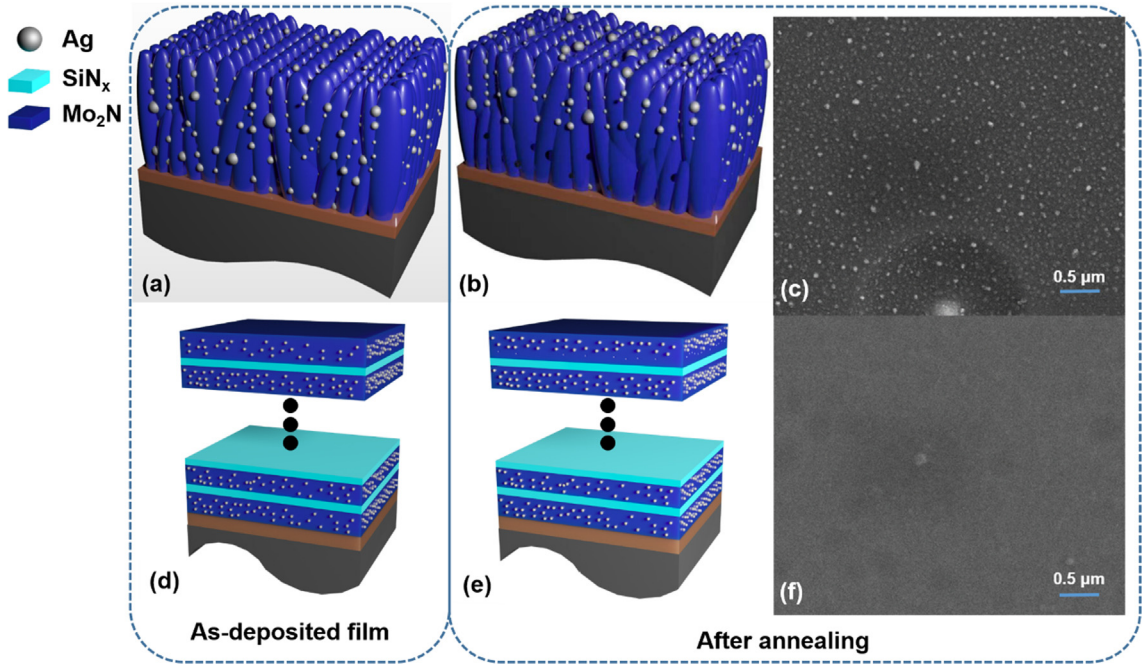

Fig. 10. Schematic representation of as-deposited (a) and annealed (b) Mo_2N-Ag monolithic film, SEM image of the Mo_2N-Ag monolithic film surface after 500 °C annealing (c), schematic representation of as-deposited (d) and annealed (e) Mo_2N-Ag/SiN_x multilayer film, and (d) SEM image of the Mo_2N-Ag/SiN_x multilayer film surface with Λ of 64 nm.

Fig. 10 illustrates the anti-diffusion of Ag in the Mo_2N by inserting amorphous SiN_x layers in a multilayer architecture. High-temperature could easily induce the excessive diffusion of nano-particles Ag in the Mo_2N-Ag monolithic film due to the large number of diffusion channels of grain boundaries, and finally leads to the premature failure, based on the schematic representation of as-deposited (Fig. 10a) and after-annealing (Fig. 10b) Mo_2N-Ag monolithic film. SEM result of the Mo_2N-Ag monolithic film surface after 500 °C annealing in the air shown in Fig. 10(c) also confirms this, and lots of white particles (Ag) are detected on the film surface. However, the deposition of the films with multilayer architecture Mo_2N-Ag/SiN_x allows in one way the growth of a more compact morphology and in the other effectively avoid the excessive diffusion of Ag in the inner of the film to the surface. Fig. 10(d) shows the SEM image of the Mo_2N-Ag/SiN_x multilayer film (Λ = 64 nm), and no obvious white particles of Ag appears. This results also demonstrates the barrier function of SiN_x layers.

Based on above tribological results, the temperature-cycling tribological properties of the multilayer films are governed by the synergistic effects between the self-lubricant Mo_2N-Ag layers and the protective SiN_x hard layers. The friction property of the multilayer films mainly influenced by three factors: (i) molybdenum nitride exhibits the excellent self-lubrication properties at RT and elevated temperatures at a cost of high WR due to the formation of layered tribo-phase of MoO_3 [35,75]. Adding silver lubricant phase into the molybdenum nitride matrix further enhances the self-lubrication properties. (ii) The Mo_2N-Ag layer, its thickness taking up 75% of the total thickness of multilayer film regardless of Λ, ensures the friction property of the whole multilayer systems under the RT-500 °C temperature-cycling conditions. This results in a stable low Cof. of ~0.5 at RT and ~0.4 at 500 °C. (iii) Soft metal such as silver could diffuse from inner to film surface through the grain boundaries at elevated temperatures. Oxygen also mainly diffuses into the film to oxidize the film through the gain boundaries at elevated temperatures. Inserting amorphous SiN_x layers into Mo_2N-Ag matrix could avoid the excessive consumption of the lubricant phases of Mo_2N and Ag, resulting in a long-term self-lubricant under RT-500 °C temperature-cycling conditions. Multilayer design by alternating deposition of Mo_2N-Ag and SiN_x modulation layers significantly enhances the RT-500 °C temperature-cycling wear resistance as well. Several could contribute for this behavior: (i) the protection mechanism of amorphous SiN_x layers could avoid the excessive consumption of the lubricant phases. (ii) the improvement on the mechanism properties of the multilayer films by the SiN_x modulation layer.

4. Conclusion

In this manuscript multilayer films of Mo_2N-Ag/ SiN_x with increasing period thickness with a fixed thickness ratio between the Mo_2N-Ag and SiN_x layers of 3:1 were deposited using RF magnetron sputtering system. The microstructure, mechanical properties and RT and RT-500 °C temperature-cycling tribological properties were investigated. The main conclusions could be summarized as follows:

(1) Two layers (Mo_2N-Ag and SiN_x) co-existed in the multilayer films. The Mo_2N-Ag layer exhibited a dual-phase of fcc-Mo_2N and fcc-Ag, and the SiN_x layer was an amorphous phase.
(2) Both room temperature (RT) lubricant and wear-resistance properties of the films were improved gradually by increasing of Λ from 8 to 64 nm, while a further increase of Λ weakened the wear-resistance properties. Mechanical properties and the synergistic effect of modulation layers were attributed to the improvement on the tribological properties at RT.
(3) Inserting the protection SiN_x layers into the Mo_2N-Ag matrix could avoid the excessive consumption of lubricant phases, and the multilayer film at Λ = 64 nm exhibited an excellent RT-500 °C temperature-cycling self-lubricant tribological

properties, with a Cof. of ~0.5 at RT, ~0.4 at 500 °C and an outstanding wear-resistance after five temperature-cycling wear tests.

Declaration of Competing Interest

The authors declare that they have no known competing financial interests or personal relationships that could have appeared to influence the work reported in this paper.

Acknowledgement

Supported by the National Natural Science Foundation of China, China (51801081, 52071159, 52171071, 52172090); Portugal National Funds through FCT project, Portugal (2021.04115); Outstanding University Young Teachers of "Qing Lan Project" of Jiangsu Province, China; Excellent Talents of "Shenlan Project" of Jiangsu University of Science and Technology, China; China Merchants Marine Scientific Research and Innovation Fund, China. Filipe Fernandes acknowledges the funding received in the aim of the projects: MCTool[21] - ref. "POCI-01-0247- FEDER-045940", CEMMPRE – ref. "UIDB/00285/2020" and SMARTLUB – ref. "POCI-01-0145-FEDER-031807".

References

[1] H. Ju, X. He, L. Yu, J. Xu, The microstructure and tribological properties at elevated temperatures of tungsten silicon nitride films, Surf. Coat. Technol. 326 (2017) 255–263.
[2] T. Wu, C. Blawert, M. Serdechnova, P. Karlova, G. Dovzhenko, D.C. Florian Wieland, S. Stojadinovic, R. Vasilic, L. Wang, C. Wang, K. Mojsilovic, M.L. Zheludkevich, Role of phosphate, silicate and aluminate in the electrolytes on PEO coating formation and properties of coated Ti6Al4V alloy, Appl. Surf. Sci. 595 (2022) 153523, https://doi.org/10.1016/j.apsusc.2022.153523.
[3] B. Huang, Q. Zhou, Q.i. An, E.-G. Zhang, Q. Chen, D.-D. Liang, H.-M. Du, Z.-M. Li, Tribological performance of the gradient composite TiAlSiN coating with various friction pairs, Surf. Coat. Technol. 429 (2022) 127945, https://doi.org/10.1016/j.surfcoat.2021.127945.
[4] H. Ju, D. Yu, J. Xu, L. Yu, B. Zuo, Y. Geng, T. Huang, L. Shao, L. Ren, C. Du, H. Zhang, H. Mao, Crystal structure and tribological properties of ZrAlMoN composite films deposited by magnetron sputtering, Mater. Chem. Phys. 230 (2019) 347–354.
[5] J. Yang, H. Fu, Y. He, Z. Gu, Y. Fu, J. Ji, Y. Zhang, Y. Zhou, Investigation on friction and wear performance of volcano-shaped textured PVD coating, Surf. Coat. Technol. 431 (2022) 128044, https://doi.org/10.1016/j.surfcoat.2021.128044.
[6] J. Kang, Y. Lu, X. Yang, X. Zhao, Y. Zhang, Z. Xing, Modeling and experimental investigation of wear and roughness for honed cylinder liner during running-in process, Tribol. Int. 171 (2022) 107531, https://doi.org/10.1016/j.triboint.2022.107531.
[7] L. Simo Kamga, D. Meffert, B. Magyar, M. Oehler, B. Sauer, Simulative investigation of the influence of surface texturing on the elastohydrodynamic lubrication in chain joints, Tribol. Int. 171 (2022) 107564, https://doi.org/10.1016/j.triboint.2022.107564.
[8] G. Vaitkunaite, C. Espejo, B. Thiebaut, A. Neville, A. Morina, Low friction tribofilm formation and distribution on an engine cylinder tested with MoDTC-containing low viscosity engine lubricants, Tribol. Int. 171 (2022) 107551, https://doi.org/10.1016/j.triboint.2022.107551.
[9] A.V. Bondarev, P.V. Kiryukhantsev-Korneev, A.N. Sheveyko, D.V. Shtansky, Structure, tribological and electrochemical properties of low friction TiAlSiCN/MoSeC coatings, Appl. Surf. Sci. 327 (2015) 253–261.
[10] D. Wu, Q. Su, L. Chen, H. Cui, Z. Zhao, Y. Wu, H. Zhou, J. Chen, Achieving high anti-wear and corrosion protection performance of phenoxy-resin coatings based on reinforcing with functional graphene oxide, Appl. Surf. Sci. 601 (2022) 154156, https://doi.org/10.1016/j.apsusc.2022.154156.
[11] Chetan, S. Ghosh, P. Venkateswara Rao, Application of sustainable techniques in metal cutting for enhanced machinability: a review, J. Cleaner Prod. 100 (2015) 17–34.
[12] G.S. Goindi, P. Sarkar, Dry machining: a step towards sustainable machining – challenges and future directions, J. Cleaner Prod. 165 (2017) 1557–1571.
[13] H. Hegab, H.A. Kishawy, B. Darras, Sustainable cooling and lubrication strategies in machining processes: a comparative study, Procedia Manuf. 33 (2019) 786–793.
[14] K. Holmberg, P. Andersson, A. Erdemir, Global energy consumption due to friction in passenger cars, Tribol. Int. 47 (2012) 221–234.
[15] S. Sartori, A. Ghiotti, S. Bruschi, Hybrid lubricating/cooling strategies to reduce the tool wear in finishing turning of difficult-to-cut alloys, Wear 376-377 (2017) 107–114.
[16] R. Li, X. Zhao, Z. Bu, Y. An, H. Zhou, W. Duan, J. Chen, Influence of different introduction modes of metal Ag into plasma sprayed Al2O3 coating on tribological properties, Ceram. Int. 48 (2022) 9286–9296.
[17] M. Ren, H. Yu, L. Zhu, H. Li, H. Wang, Z. Xing, B. Xu, Microstructure, mechanical properties and tribological behaviors of TiAlN-Ag composite coatings by pulsed magnetron sputtering method, Surf. Coat. Technol. 436 (2022) 128286.
[18] H. Ju, N. Ding, J. Xu, L. Yu, Y. Geng, F. Ahmed, The tribological behavior of niobium nitride and silver composite films at elevated testing temperatures, Mater. Chem. Phys. 237 (2019).
[19] A.V. Bondarev, D.G. Kvashnin, I.V. Shchetinin, D.V. Shtansky, Temperature-dependent structural transformation and friction behavior of nanocomposite VCN-(Ag) coatings, Mater. Des. 160 (2018) 964–973.
[20] M. Zhang, F. Zhou, Y. Wu, Q. Wang, Z. Zhou, Microstructure and electrochemical characteristics of CrMoN/Ag nanocomposite coatings in seawater, Surf. Coat. Technol. 441 (2022) 128551.
[21] D. Geng, H. Li, Z. Chen, Y. Xu, Q. Wang, Microstructure, oxidation behavior and tribological properties of AlCrN/Cu coatings deposited by a hybrid PVD technique, J. Mater. Sci. Technol. 100 (2022) 150–160.
[22] Q. Li, N. Zhang, Y. Gao, Y. Qing, Y. Zhu, K. Yang, J. Zhu, H. Wang, Z. Ma, L. Gao, Y. Liu, J. He, Effect of the core-shell structure powders on the microstructure and thermal conduction property of YSZ/Cu composite coatings, Surf. Coat. Technol. 424 (2021) 127658.
[23] H. Mei, J. Ding, Z. Zhao, Q. Li, J. Song, Y. Li, W. Gong, F. Ren, Q. Wang, Effect of Cu content on high-temperature tribological properties and oxidation behavior of Al-Ti-V-Cu-N coatings deposited by HIPIMS, Surf. Coat. Technol. 434 (2022) 128130.
[24] X. Luo, D. Ma, P. Jing, Y. Gong, Y. Zhang, F. Jing, Y. Leng, In vitro analysis of cell compatibility of TiCuN films with different Cu contents, Surf. Coat. Technol. 408 (2021) 126790.
[25] S. Tan, X. Zhang, X. Wu, F. Fang, J. Jiang, Comparison study on structure of Si and Cu doping CrN films by reactive sputtering, Appl. Surf. Sci. 257 (2011) 5595–5600.
[26] H. Ju, N. Ding, J. Xu, L. Yu, Y. Geng, G. Yi, T. Wei, Improvement of tribological properties of niobium nitride films via copper addition, Vacuum 158 (2018) 1–5.
[27] A.D. Pogrebnjak, A.A. Bagdasaryan, A. Pshyk, K. Dyadyura, Adaptive multicomponent nanocomposite coatings in surface engineering, Phys. Usp. 60 (2017) 586–607.
[28] H. Ju, N. Ding, J. Xu, L. Yu, Y. Geng, F. Ahmed, B. Zuo, L. Shao, The influence of crystal structure and the enhancement of mechanical and frictional properties of titanium nitride film by addition of ruthenium, Appl. Surf. Sci. 489 (2019) 247–254.
[29] Y. Wang, L. Guan, Z. He, S. Zhang, H. Singh, M.D. Hayat, C. Yao, Influence of pretreatments on physicochemical properties of Ni-P coatings electrodeposited on aluminum alloy, Mater. Des. 197 (2021) 109233.
[30] H. Ju, L. Yu, S. He, I. Asempah, J. Xu, Y. Hou, The enhancement of fracture toughness and tribological properties of the titanium nitride films by doping yttrium, Surf. Coat. Technol. 321 (2017) 57–63.
[31] X. Dai, M. Wen, K. Huang, X. Wang, L. Yang, J. Wang, K. Zhang, Toward low friction in water for Mo2N/Ag coatings by tailoring the wettability, Appl. Surf. Sci. 447 (2018) 886–893.
[32] D.V. Shtansky, A.V. Bondarev, P.V. Kiryukhantsev-Korneev, T.C. Rojas, V. Godinho, A. Fernández, Structure and tribological properties of MoCN-Ag coatings in the temperature range of 25–700°C, Appl. Surf. Sci. 273 (2013) 408–414.
[33] M. Zhang, F. Zhou, Y. Fu, Q. Wang, Z. Zhou, Influence of Ag target current on the structure and tribological properties of CrMoSiCN/Ag coatings in air and water, Tribol. Int. 160 (2021) 107059.
[34] R. Zhou, H. Ju, S. Liu, Z. Zhao, J. Xu, L. Yu, H. Qian, S. Jia, R. Song, J. Shen, The influences of Ag content on the friction and wear properties of TiCN–Ag films, Vacuum 196 (2022) 110719.
[35] H. Ju, R. Zhou, S. Liu, L. Yu, J. Xu, Y. Geng, Enhancement of the tribological behavior of self-lubricating nanocomposite Mo2N/Cu films by adding the amorphous SiNx, Surf. Coat. Technol. 423 (2021) 127565.
[36] H. Ju, D. Yu, L. Yu, N. Ding, J. Xu, X. Zhang, Y. Zheng, L. Yang, X. He, The influence of Ag contents on the microstructure, mechanical and tribological properties of ZrN-Ag films, Vacuum 148 (2018) 54–61.
[37] S.K. Ghosh, C. Miller, G. Perez, H. Carlton, D. Huitink, S. Beckford, M. Zou, Effect of Cu nanoparticles on the tribological performance of polydopamine + polytetrafluoroethylene coatings in oil-lubricated condition, Appl. Surf. Sci. 565 (2021) 150525.
[38] Q. Wang, M. Zhou, F. Zhou, Z. Zhou, X. Jin, The toughness evaluation of CrBN coatings doped with Ni or Cu by experiment and FEM, Appl. Surf. Sci. 599 (2022) 153804.
[39] A. Al-Rjoub, A. Cavaleiro, F. Fernandes, Influence of Ag alloying on the morphology, structure, mechanical properties, thermal stability and oxidation resistance of multilayered TiSiN/Ti(Ag)N films, Mater. Des. 192 (2020) 108703.
[40] A. Al-Rjoub, A. Cavaleiro, T.B. Yaqub, M. Evaristo, N.M. Figueiredo, F. Fernandes, TiAlSiN(Ag) coatings for high temperature applications: the influence of Ag alloying on the morphology, structure, thermal stability and oxidation resistance, Surf. Coat. Technol. 442 (2022) 128087.
[41] S.S. Rajput, S. Gangopadhyay, A. Cavaleiro, A. Al-Rjoub, C.S. Kumar, F. Fernandes, Influence of Ag additions on the structure, mechanical properties and oxidation behaviour of CrAlNAg coatings deposited by sputtering, Surf. Coat. Technol. 426 (2021) 127767.

[42] A.D. Pogrebnjak, K. Smyrnova, O. Bondar, Nanocomposite multilayer binary nitride coatings based on transition and refractory metals: structure and properties, Coatings 9 (2019).
[43] Z. Yang, J. Zhu, Y. Zhu, H. Luo, Z. Li, H. Jiang, L. Zhao, Asymmetric interface and growth mechanism in sputtered W/Si and WSi2/Si multilayers, Appl. Surf. Sci. (2022) 154531.
[44] Y. He, X. Wang, T. Guo, K. Gao, X. Pang, Crystal interface-enhanced thermal stability of CrAlN/SiNx multilayer films, Surf. Coat. Technol. 445 (2022) 128725.
[45] F. Frank, C. Kainz, M. Tkadletz, C. Czettl, M. Pohler, N. Schalk, Microstructural and micro-mechanical investigation of cathodic arc evaporated ZrN/TiN multilayer coatings with varying bilayer thickness, Surf. Coat. Technol. 432 (2022) 128070.
[46] J. Chen, Z. Zhang, G. Yang, Z. Fang, Z. Yang, Z. Li, G. He, Performance and damage mechanism of TiN/ZrN nano-multilayer coatings based on different erosion angles, Appl. Surf. Sci. 513 (2020) 145457.
[47] C. Chang, C. Huang, C. Lin, F. Yang, J. Tang, Mechanical properties of amorphous and crystalline CrN/CrAlSiN multilayer coating fabricated using HPPMS, Surf. Interfaces 31 (2022) 102064.
[48] T. Rajabi, M. Atapour, H. Elmkhah, S.M. Nahvi, Nanometric CrN/CrAlN and CrN/ZrN multilayer physical vapor deposited coatings on 316L stainless steel as bipolar plate for proton exchange membrane fuel cells, Thin Solid Films 753 (2022) 139288.
[49] A.D. Pogrebnjak, V.M. Beresnev, O.V. Bondar, B.O. Postolnyi, K. Zaleski, E. Coy, S. Jurga, M.O. Lisovenko, P. Konarski, L. Rebouta, J.P. Araujo, Superhard CrN/MoN coatings with multilayer architecture, Mater. Des. 153 (2018) 47–59.
[50] J.J. Hu, C. Muratore, A.A. Voevodin, Silver diffusion and high-temperature lubrication mechanisms of YSZ–Ag–Mo based nanocomposite coatings, Compos. Sci. Technol. 67 (2007) 336–347.
[51] C. Muratore, J.J. Hu, A.A. Voevodin, Tribological coatings for lubrication over multiple thermal cycles, Surf. Coat. Technol. 203 (2009) 957–962.
[52] A. Gupta, X-ray and neutron studies of nanoscale atomic diffusion in thin films and multilayers, Appl. Surf. Sci. 256 (2009) 552–557.
[53] J. Ni, X. Zhao, J. Zhao, P-type transparent conducting SnO2: Zn film derived from thermal diffusion of Zn/SnO2/Zn multilayer thin films, Surf. Coat. Technol. 206 (2012) 4356–4361.
[54] X. Hu, L. Qiu, X. Pan, J. Zhang, X. Li, S. Zhang, C. Dong, Nitrogen diffusion mechanism, microstructure and mechanical properties of thick Cr/CrN multilayer prepared by arc deposition system, Vacuum 199 (2022) 110902.
[55] V. Lenzi, A. Cavaleiro, F. Fernandes, L. Marques, Diffusion of silver in titanium nitride: insights from density functional theory and molecular dynamics, Appl. Surf. Sci. 556 (2021) 149738.
[56] X. Dai, M. Wen, J. Wang, X. Cui, X. Wang, K. Zhang, The tribological performance at elevated temperatures of MoNbN-Ag coatings, Appl. Surf. Sci. 509 (2020) 145372.
[57] D. Zhao, S. Li, X. Zhao, E. Hao, Y. An, H. Zhou, J. Chen, Preparation and vacuum tribological properties of composite coatings fabricated by effective introduction of soft metal Ag into spray-formed YSZ templates, Appl. Surf. Sci. 518 (2020) 146176.
[58] X. Bai, J. Li, L. Zhu, L. Wang, Effect of Cu content on microstructure, mechanical and anti-fouling properties of TiSiN-Cu coating deposited by multi-arc ion plating, Appl. Surf. Sci. 427 (2018) 444–451.
[59] Y. Wang, J. Chen, Y. Yang, Z. Liu, H. Wang, Z. He, Nanostructured superhydrophobic titanium-based materials: a novel preparation pathway to attain superhydrophobicity on TC4 alloy, Nanomaterials 12 (2022) 2086.
[60] Y. Wang, L. Guan, Z. He, J. Tan, H. Singh, M. Hayat, C. Yao, Preparation and characterization of AAO/Ni/Ni superhydrophobic coatings on aluminum alloys, Surf. Eng. 10 (2021) 1246–1254.
[61] X. Xu, F. Su, Z. Li, Microstructure and tribological behaviors of MoN-Cu nanocomposite coatings sliding against Si3N4 ball under dry and oil-lubricated conditions, Wear 434–435 (2019) 202994.
[62] X. Xu, J. Sun, F. Su, Z. Li, Y. Chen, Z. Xu, Microstructure and tribological performance of adaptive MoN–Ag nanocomposite coatings with various Ag contents, Wear 488–489 (2022) 204170.
[63] M. Hu, X. Gao, J. Sun, L. Weng, F. Zhou, W. Liu, The effects of nanoscaled amorphous Si and SiNx protective layers on the atomic oxygen resistant and tribological properties of Ag film, Appl. Surf. Sci. 258 (2012) 5683–5688.
[64] S. Balamurugan, N. Naresh, I. Prakash, N. Satyanarayana, Capacity fading mechanism of Li2O loaded NiFe2O4/SiO2 aerogel anode for lithium-ion battery: ex-situ XPS analysis, Appl. Surf. Sci. 535 (2021) 147677.
[65] N. Esfandiari, M. Kashefi, M. Mirjalili, S. Afsharnezhad, Role of silica mid-layer in thermal and chemical stability of hierarchical Fe3O4-SiO2-TiO2 nanoparticles for improvement of lead adsorption: kinetics, thermodynamic and deep XPS investigation, Mater. Sci. Eng., B 262 (2020) 114690.
[66] H. Ju, L. Yu, D. Yu, I. Asempah, J. Xu, Microstructure, mechanical and trobological properties of TiN-Ag films deposited by reactive magnetron sputtering, Vacuum 141 (2017) 82–88.
[67] M. Danek, F. Fernandes, A. Cavaleiro, T. Polcar, Influence of Cr additions on the structure and oxidation resistance of multilayered TiAlCrN films, Surf. Coat. Technol. 313 (2017) 158–167.
[68] H. Ju, R. Wang, N. Ding, L. Yu, J. Xu, F. Ahmed, B. Zuo, Y. Geng, Improvement on the oxidation resistance and tribological properties of molybdenum disulfide film by doping nitrogen, Mater. Des. 186 (2020) 108300.
[69] H. Ju, R. Wang, W. Wang, J. Xu, L. Yu, H. Luo, The microstructure and tribological properties of molybdenum and silicon nitride composite films, Surf. Coat. Technol. 401 (2020) 126238.
[70] D. Wang, H. Tan, W. Chen, S. Zhu, J. Cheng, J. Yang, Tribological behavior of Ni3Al–Ag based self-lubricating alloy with Ag2MoO4 formed by high temperature tribo-chemical reaction, Tribol. Int. 153 (2021) 106659.
[71] P. Dašić, F. Franek, E. Assenova, M. Radovanović, International standardization and organizations in the field of tribology, Ind. Lubr. Tribol. 55 (2013) 287–291.
[72] H.P. Jost, Tribology micro & macro economics: a road to economic savings, Lubr. Eng. 61 (2005) 18–22.
[73] O. Hod, E. Meyer, Q. Zheng, M. Urbakh, Structural superlubricity and ultralow friction across the length scales, Nature 563 (2018) 485–492.
[74] P. Zhang, S. Li, Z. Zhang, General relationship between strength and hardness, Mater. Sci. Eng., A 529 (2011) 62–73.
[75] C. Liu, H. Ju, J. Xu, L. Yu, Z. Zhao, Y. Geng, Y. Zhao, Influence of copper on the compositions, microstructure and room and elevated temperature tribological properties of the molybdenum nitride film, Surf. Coat. Technol. 395 (2020) 125811.